Supporting Online Material

Materials and Methods

Vectors and Viral infections

The following retroviral vectors were used in this study: pLNCX2-Neo (ER:H-*ras*V12, encoding a fusion protein of the estrogen receptor ligand-binding domain and H-rasV12), and pLPC-Puro (*Flag-RAGB T54N*, *mRFP-GFP-LC3*). *HA-ULK1*/pMXs-IP was a generous gift from Noboru Mizushima (Tokyo Medical and Dental University, Tokyo, Japan). The *mRFP-GFP-LC3* cDNA was a generous gift from Kevin Ryan (Cancer Research UK, Beatson Institute, Glasgow, UK) and was sub-cloned into pLPC. Retroviral gene transfer was performed as described (*1*). CellLight Golgi-GFP (BacMam 2.0) and Premo Autophagy Sensor LC3B-RFP (BacMam 2.0) were purchased from Invitrogen.

Cell lines and tissue culture

IMR90 human diploid fibroblasts and HL60 cells were purchased from the ATCC and were cultured in DMEM (phenol red-free) and RPMI 1640, respectively, supplemented with 10% FBS and antibiotics. IMR90 cells were maintained at 5% oxygen, except for the microarray experiments. HL60 cells were maintained at atmospheric oxygen levels. To induce senescence, IMR90 cells expressing ER:H-*Ras*V12 (ER:Ras-IMR90 cells) were given 100 nM 4-hydroxytamoxifen (4OHT) (*2*). HL60 cells were induced to differentiate into macrophages using 30 nM 12-O-tetradecanoylphorbol-13-acetate

(TPA). The essential amino acid mix used in Fig. 4C was MEM amino acids (Invitrogen). To inhibit MEK activity, 50μM PD98059 (Merck) was added daily to IMR90 cells.

Immunofluoresence and senescence associated-β-galactosidase activity

Indirect immunofluorescence was performed as described (*1*). Cells were fixed in 4% paraformaldehyde in PBS for 15 min at room temperature, except for α-tubulin and RM130 staining, where cells were fixed with methanol for 7 min at -20ºC. After fixation, cells were immunolabeled using the following primary antibodies: anti-ATG12 (#2010, Cell Signaling); anti-GM130 (610823, BD Biosciences); anti-HA (H9658, Sigma); anti-IL6 & IL8 (MAB2061 & MAB208, R&D systems); anti-LAMP2 (555803, BD Biosciences); anti-LC3 (0231-100/LC3-5F10, Nanotools); anti-p62 (610832, BD Biosciences & 25575, Santa Cruz); anti-RM130 (a generous gift from Rosa Rios); anti-RagB (HPA003734, Sigma Prestige); anti-RagC (#3360, Cell Signaling); anti-TGN46 (AHP500, AbD Serotec); anti-mTOR (#2983, Cell Signaling); anti-α-tubulin (T5168/B-5-1-2, Sigma). Alexa Fluor 488, 555, 594 and 647 conjugates (Molecular Probes) were the secondary antibodies. DNA was visualized using 4',6-diamidino-2-phenylindole (DAPI) (1 μg/ml). Senescence associated-β-galactosidase activity was detected as described (*1*). For TASCC counting; areas with a diameter of roughly 3μm or greater were counted as positive.

Electron Microscopy

Electron microscopy was performed as reported (*3*). Briefly, cells were fixed by a conventional method (1.5% paraformaldehyde and 3% glutaraldehyde in 0.1 M

phosphate buffer, pH 7.3, followed by an aqueous solution of 1% OsO_4). Fixed samples were embedded in Epon 812 and thin sections (70-80 nm) were then cut and stained with uranyl acetate and lead citrate for observation under a JEOL-1010 electron microscope (JEOL) at 80 kV. For correlative fluorescence-EM, LC3 (RFP) and Golgi (GFP) were labeled by Premo Autophagy Sensor and CellLight (BacMam 2.0, Invitrogen), respectively. Cells were plated on grided coverslips, and fixed with paraformaldehyde and glutaraldehyde. After acquisition of fluorescent images using a Leica DMI6000B epi-fluorescence light microscope, cells were treated with OsO_4. The grids were used for the identification of cells in the subsequent EM analyses.

mRNA fluorescence *in situ* hybridization (FISH)

mRNA FISH was performed using a QuantiGene ViewRNA assay kit (Panomics) according to the manufacturer's recommendations. The human *IL8* probe was purchased from Panomics.

Nascent protein detection

To visualize nascent proteins, we used Click-iT reagents (Invitrogen). Cells were incubated in methionine-free medium for 30 min prior to the addition of the methionine analog L-homopropargylglycine (HPG) for 3 or 30 min. Pulse-chase experiments were also performed: after a 30 min incubation with HPG (pulse), the cells were washed, followed by a 90 min incubation with normal methionine (chase). After washing with cold PBS, cells were pre-extracted with 0.0625% saponin in cold CSK buffer (100 mM NaCl, 300 mM sucrose, 3 mM $MgCl_2$, 10 mM PIPES (NaOH) pH 6.8) on ice for 3 min

followed by fixation with 4% paraformaldehyde for 15 min. The Click-iT reaction, with Alexa-488 detection reagents, was performed according to the manufacture's protocol. For the control experiment, to confirm the specificity of the signal, 25μM cycloheximide (Sigma), a protein synthesis inhibitor, was added 30 min before HPG addition. After the Click-iT reaction, cells were subjected to IF analysis as described above.

Brefeldin A and nocodazole treatment

To assess the acute impact of Nocodazole (NZ) or Brefeldin A (BFA) on the TASCC, day 4 senescent cells were incubated with 10 μM NZ or 40 ng/ml BFA for 2 h. While this experiment was focused on the maintenance of the TASCC structure, in order to test whether NZ or BFA prevents TASCC formation, the drugs had to be added before TASCC formation was induced. Therefore we added NZ or BFA together with 4OHT, and cells were assessed for TASCC formation after 24 h by immunofluorescence for mTOR and LAMP2. To confirm the reversibility of the BFA effect after 24 h treatment, cells were washed and chased with fresh BFA-free medium (which was otherwise the same) for an additional 2 h. Reformation of the Golgi apparatus was assessed by immunofluorescence of RM130.

Cell Viability

Cells (1×10^5) were plated into 12-well plates 24 h before treatment. After 24 h treatment with 10 μM Nocodazole (NZ) or 40 ng/ml Brefeldin A (BFA), adherent and non-adherent cells were pooled and analyzed for viability by trypan blue exclusion.

Gene expression

Immunoblotting analysis was carried out as described (*2*). For HL60 cells, both suspended and attached cells were collected. Blots were probed with the following antibodies: anti-ß-actin (A5441, Sigma); anti-CD11b (ab52478, Abcam); anti-4E-BP1 (#9644, Cell Signaling); anti-phospho-4E-BP1 (#9459, Cell Signaling); anti-IL6 & IL8 (MAB2061 & MAB208, R&D systems); anti-LC3 (0231-100/LC3-5F10, Nanotools); anti-p62 (610832, BD Biosciences); anti-phospho-p70S6K (Thr389) (#9206, Cell Signaling); total-p70S6K (#9202, Cell Signaling); anti-RagB (HPA003734, Sigma Prestige); anti-RagC (#3360, Cell Signaling); anti-H-Ras (OP23, Calbiochem / Merck). Quantitative RT-PCR was performed as described (*2, 4*). Primers for *IL6*, *IL8,* and *β-Actin* (internal control) were:

IL6 Forward: TGAAAGCAGCAAAGAGGCACTG

IL6 Reverse: TGAATCCAGATTGGAAGCATCC

IL8 Forward: AAGGAAAACTGGGTGCAGAG

IL8 Reverse: ATTGCATCTGGCAACCCTAC

β-Actin Forward: TTCAACACCCCAGCCATGT

β-Actin Reverse: GCCAGTGGTACGGCCAGA

The primer sets for the lysosomal genes were described previously (*5*).

For microarray experiments, cRNA was hybridized to Human-6 v2 Expression BeadChips (Illumina) as per the manufacturer's instructions. Three biological replicates were performed for each time point. The bead-level data were preprocessed and analyzed

using the R beadarray package (*6*).

Gene Ontology (GO) analysis

Microarray analysis identified differentially expressed genes ($\log_2$ ratio ≥ 0.58 or ≤ -0.58 and False Discovery Rate (FDR) adjusted P-value ≤ 0.01) at day 4 in Ras-induced senescent IMR90 cells. Upregulated genes (compared to day 0) were used for functional analysis, while Illumina Human-6 v2 was used as the background set. GO analysis was performed using the web-based NIH DAVID v6.7 software (*7*). Gene lists were analyzed using a medium cut off and enrichment score ≥ 1 and a P-value ≤ 0.01 was used to identify over-represented ontologies. Ontology networks were further investigated and visualized using Cytoscape v2.6.3 software (*8*) and the associated Cluego (*9*) and Bingo (*10*) modules.

Lysosomal Gene analysis

Literature sources, including a lysosomal proteomic dataset (*11*) and Ingenuity Pathway Analysis v8.6 software (Ingenuity Systems, www.ingenuity.com), were used to identify and visualize genes involved in lysosome biogenesis and functions.

Protein solubility assay

Cells were resuspended in lysis buffer (40 mM HEPES pH 7.4, 120 mM NaCl 1 mM EDTA, 1% Triton X-100, 1 mM PMSF, and PhosSTOP & EDTA-free Complete tablet (Roche)). After 30 min incubation on ice, the lysates were separated into soluble (supernatant) and insoluble (pellet) fractions by centrifugation at 14,000 rpm for 10 min

in a microfuge. The pellets were re-suspended with 1x Laemmli buffer.

Immunohistochemistry

Immunohistochemical staining was performed on paraffin-embedded renal cortex tissues. For paraffin-embedded tissue, the renal tissues from 4-week-old C57BL/6J (Jackson laboratory) were fixed by trans-cardiac perfusion with phosphate saline buffer (PBS) containing 4% paraformaldehyde. Papillomas were generated and analyzed as described *(12)*. Staining was visualized by indirect immunofluorescence or DAB. The following antibodies were used: anti-mTOR (#2983, Cell Signaling); anti-Lamp2 (ab13524, Abcam); anti-LC3 (0231-100/LC3-5F10, Nanotools); anti-GM130 (610823, BD Biosciences); anti-WT1 (C-19, Santa Cruz); anti-VEGF (ab46154, Abcam); anti-DEC1 (generous gift from Adrian Harris, Molecular Oncology Laboratories, University Department of Medical Oncology, Weatherall Institute of Molecular Medicine, John Radcliffe Hospital, Oxford, UK) *(13)*.

References for Materials and Methods

1. M. Narita *et al*., *Cell* **126**, 503 (2006).
2. A. R. J. Young *et al*., *Genes Dev.* **23**, 798 (2009).
3. Y. Nishida *et al*., *Nature* **461**, 654 (2009).
4. J. Acosta *et al*., *Cell* **133**, 1006 (2008).
5. M. Sardiello *et al*., *Science* **325**, 473 (2009).
6. M. J. Dunning, M. L. Smith, M. E. Ritchie, S. Tavare, *Bioinformatics* **23**, 2183 (2007).
7. W. Huang da, B. T. Sherman, R. A. Lempicki, *Nat. Protoc.* **4**, 44 (2009).
8. P. Shannon *et al*., *Genome Res.* **13**, 2498 (2003).
9. G. Bindea *et al*., *Bioinformatics* **25**, 1091 (2009).
10. S. Maere, K. Heymans, M. Kuiper, *Bioinformatics* **21**, 3448 (2005).
11. T. Lubke, P. Lobel, D. E. Sleat, *Biochim. Biophys. Acta* **1793**, 625 (2009).
12. D.M. Owens, F.M. Watt, *Cancer Res.* **61**, 5248 (2001).
13. A. Giatromanolaki, *et al*., *J. Pathol.* **200**: 222 (2003).

Supplemental fig. S1

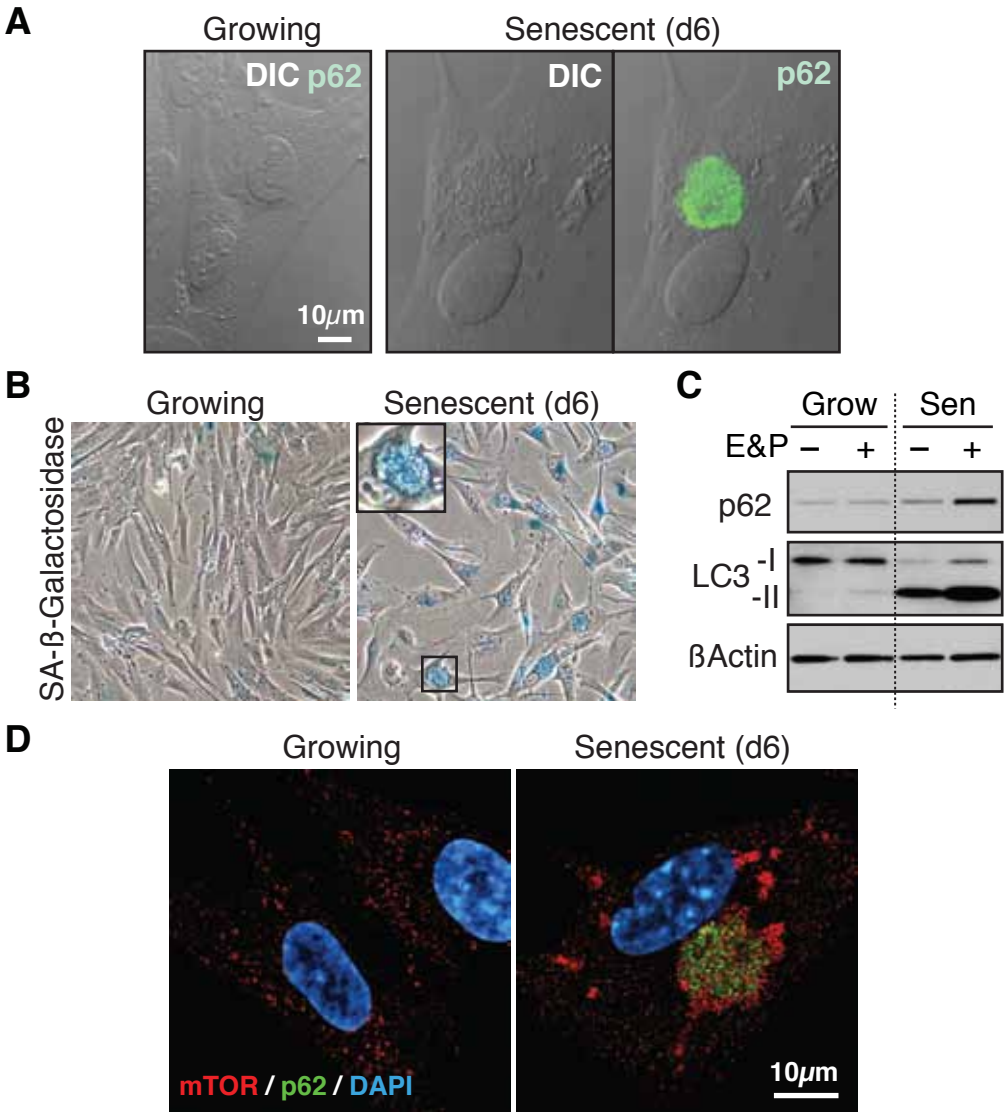

fig. S1. Senescence-associated cytoplasmic compartments.
(**A**) Overlaid confocal microscopy images of p62 immunofluorescence and the corresponding DIC image in the cells indicated. ER:Ras-IMR90 cells were given no (Growing) or 4OHT for 6 days (Senescent). (**B**) Senescence associated-β-galactosidase activity (blue). The inset shows a magnified image of the cell indicated by the square. (**C**) Autophagic flux is intact during Ras-induced senescence (Sen). Immunoblot analysis for the indicated proteins is shown. E&P, 10 μg/ml E64d and 25 μg/ml Pepstatin A (lysosomal protease inhibitors) were added 3 hours before extraction. Both p62 and LC3-II levels are further increased by inhibiting lysosomal proteases in senescent cells. (**D**) Confocal images of indirect immunofluorescence for mTOR and p62 in the cells indicated. Note, this compartment was consistently absent in cells expressing both Ras and E1A, an adenoviral oncoprotein that completely blocks Ras-induced senescence.

Supplemental fig. S2

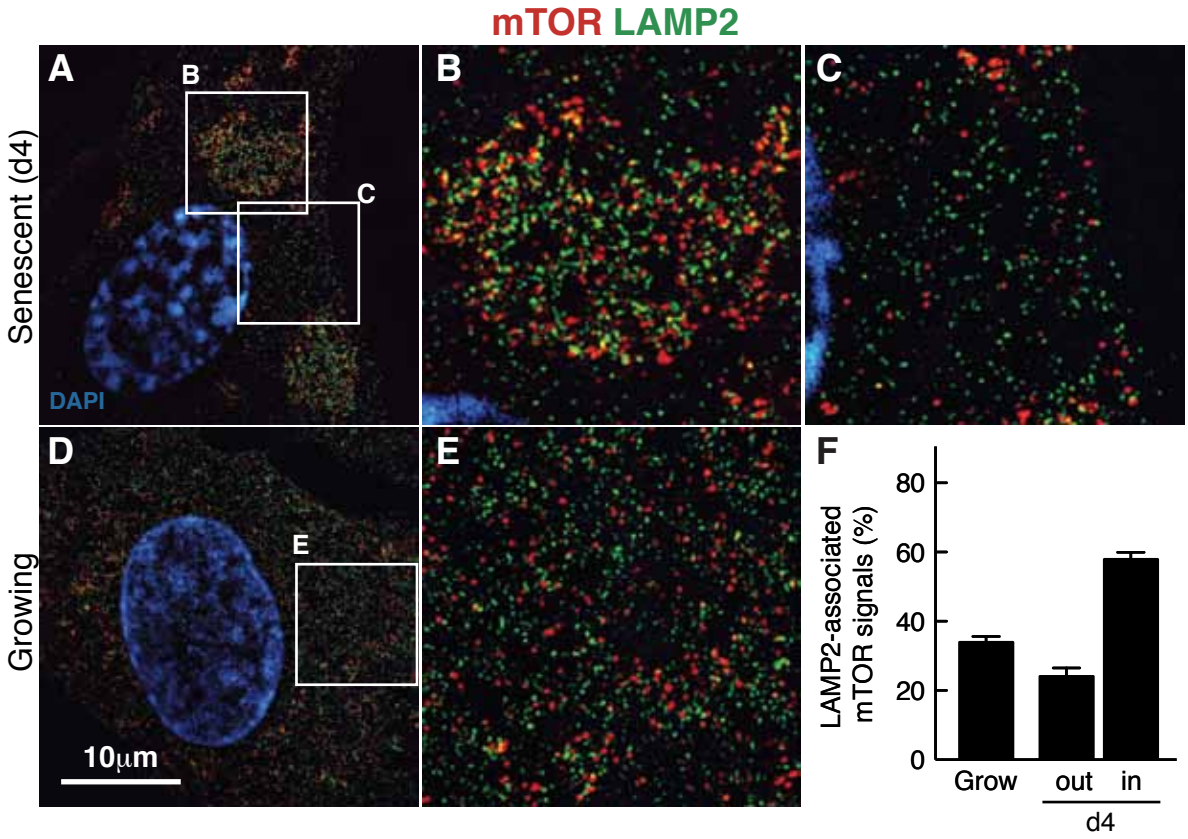

fig. S2. Spatial association of mTOR with lysosomes.
(**A** to **E**) High-resolution immunofluorescence images produced by Structured Illumination Microscopy on the DeltaVision OMX 3D SIM Super-resolution microscope. mTOR (red) and LAMP2 (green) were labelled in day 4 Ras-induced senescent (A) and growing (D) IMR90 cells. The regions indicated by the squares are magnified in the corresponding panels (B, C, and E). While A, B and D are processed using identical conditions, the contrast in C and E is slightly enhanced to enable a better view of the spatial relationship between the green and red signals. (**F**) mTOR signals that were associated with LAMP2 signals were assessed within (in) or outside (out) the mTOR-LAMP2 enriched compartments in day 4 senescent cells using z-stack images (step size: 125nm). Growing cells serve as a control, showing an intermediate value between 'in' and 'out'. At least 10 TASCC-positive or normal growing cells were chosen from two different preparations, and isolated and LAMP2-associated 'mTOR-dots' were counted in each area.

Supplemental fig. S3

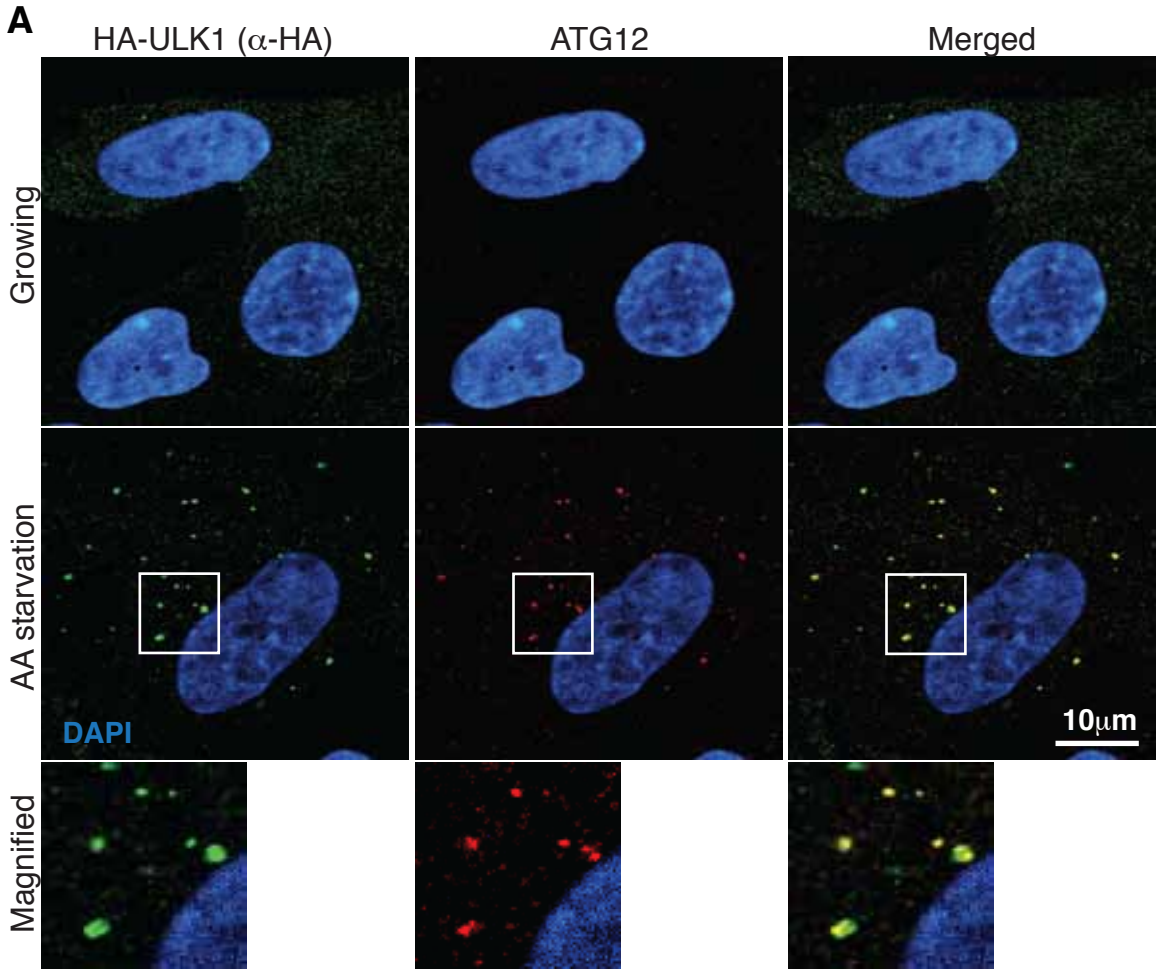

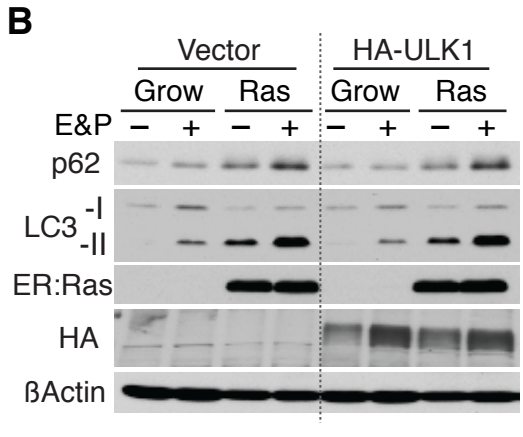

fig. S3. Assessment of ATG12 and HA (-ULK1) immunofluorescence (IF).
(**A**) HA-ULK1 and endogenous ATG12 colocalize in puncta induced by amino acid (AA) starvation in IMR90 cells. (**B**) Autophagy flux is intact in HA-ULK1 expressing IMR90 cells. HA-ULK1 or control vector expressing ER:Ras-IMR90 cells were given no (Grow) or 4OHT for 4 days (Ras). E&P, 10 μg/ml E64d and 25 μg/ml Pepstatin A (lysosomal protease inhibitors) were added 3 hours before extraction. Both p62 and LC3-II levels are further increased by inhibiting lysosomal proteases in both vector and HA-ULK1 expressing cells, thus this level of exogenous ULK1 did not inhibit autophagy.

Supplemental fig. S4

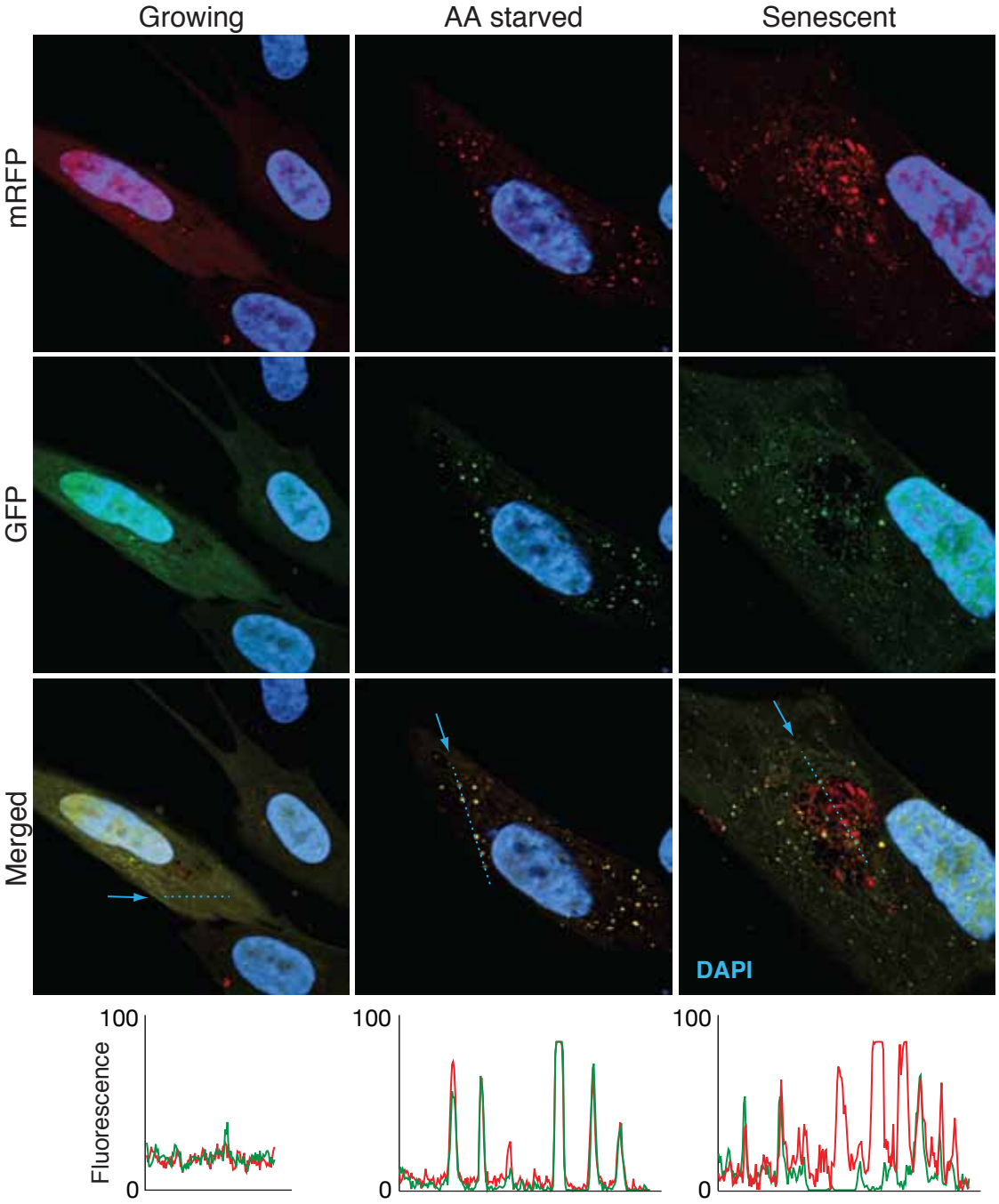

fig. S4. The TASCC is enriched for autolysosomes.
Confocal images of tandem fluorescent mRFP-GFP-LC3 in growing, amino acid (AA) starved, and Ras-induced senescent (day 4) IMR90 cells. Intensity profiles corresponding to the indicated dashed lines (arrows) are plotted for both fluorescent channels.

Supplemental fig. S5

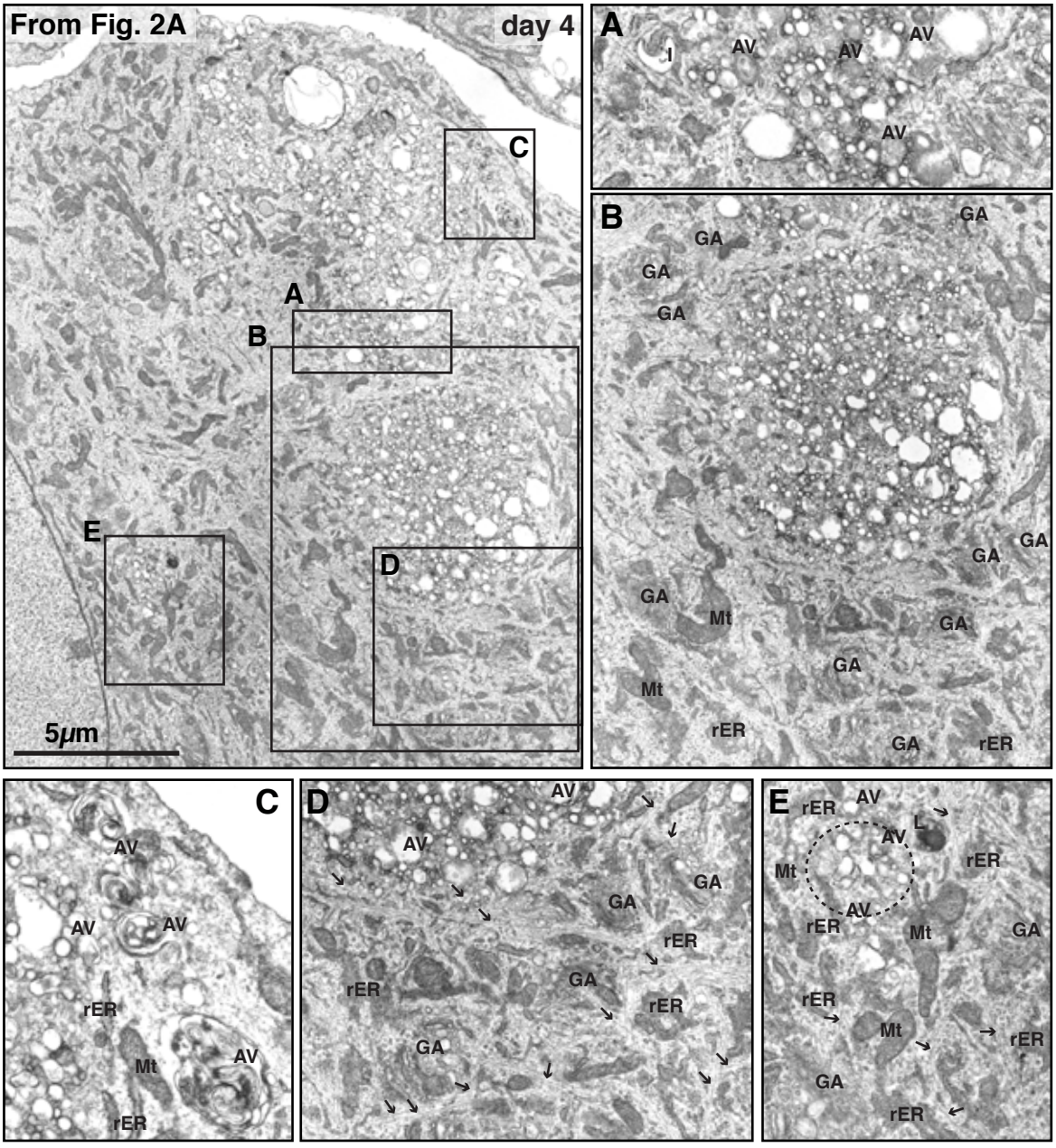

fig. S5. High magnification electron microscopy images of Ras-induced senescent IMR90 cells (from Fig. 2A).

Enlargements of the areas outlined in EM Fig. 2A are shown, corresponding to the lettered boxes indicated. (**A**) Isolation membrane (I) and autophagic vacuoles (AVs) are shown. (**B**) Compartment surrounded by many Golgi apparatus (GA). (**C**) Typical AVs are shown. (**D**) Prominent microtubules (arrows) are shown in the vicinity of the compartment. (**E**) A small compartment (dashed circle) is surrounded by lysosome (L), rER, and GA. rER, rough Endoplasmic Reticulum; Mt, mitochondria.

Supplemental fig. S6

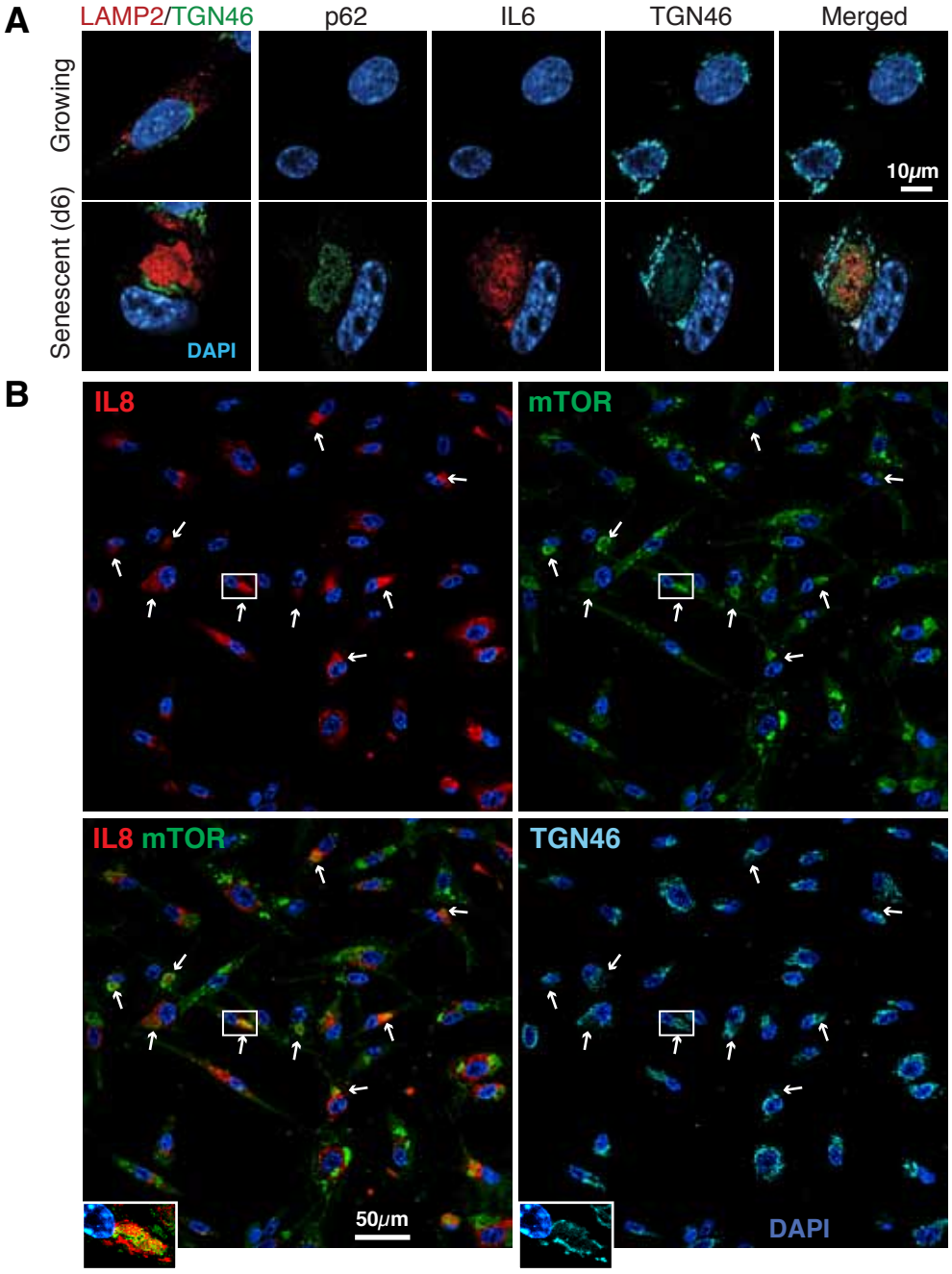

81.3 +/- 3.2 % (SEM; n=4) of TASCC (mTOR) were spatially associated with TGN.

fig. S6. Spatial association between TASCC and *trans*-Golgi network.
(**A**) Confocal immunofluorescence for indicated proteins in growing and Ras-induced senescent cells. (**B**) Lower magnification confocal images of immunofluorescence for the proteins indicated in senescent cells are shown. Arrows indicate the TASCCs, which colocalize to IL8. Most cells express IL8, which colocalizes to the TASCC and/or TGN46. A representative TASCC, which is spatially associated with the TGN (indicated by the rectangle) is magnified.

Supplemental fig. S7

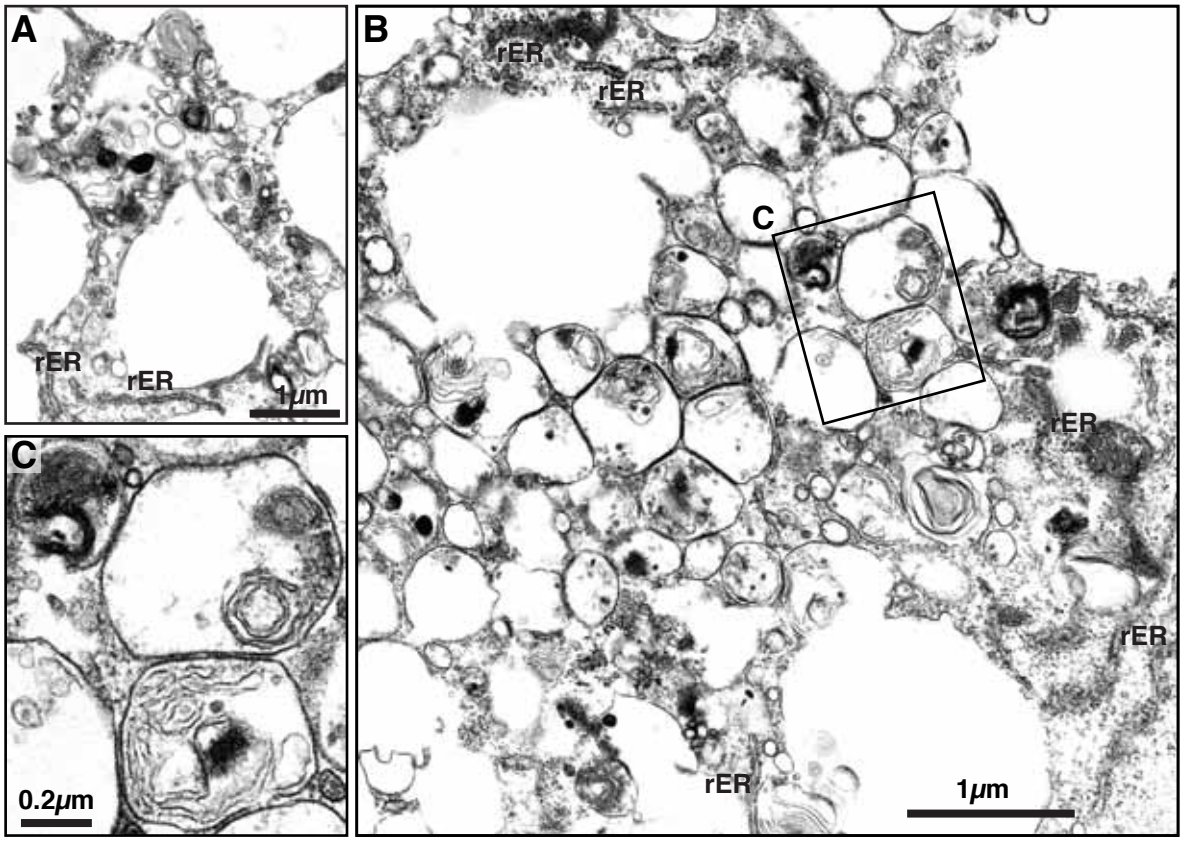

fig. S7. High magnification images from LC3 enriched regions in correlative fluorescence-EM image (from Fig. 2B).
(**A** and **B**) Magnified images from the corresponding regions indicated by the rectangles in Fig. 2B. Rough Endoplasmic Reticulum (rER) is often located around large vacuoles. (**C**) Typical image of autophagic vacuoles magnified from (B).

Supplemental fig. S8

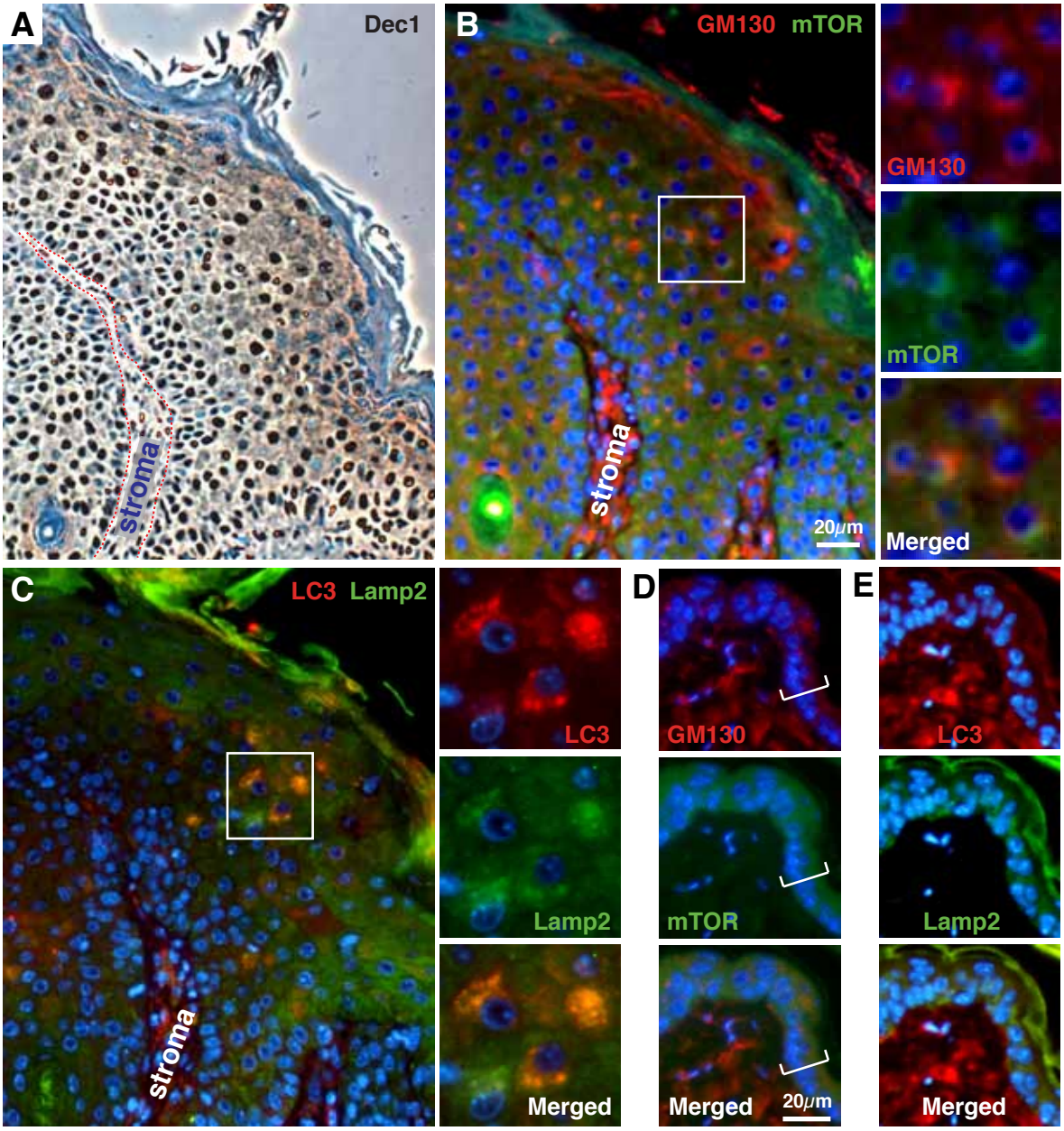

fig. S8. TASCC formation in mouse papillomas.
(**A** to **C**) Representative immunohistochemical images of serially sectioned DMBA/TPA-induced mouse papillomas, which commonly harbor a constitutively active mutation of H-*ras*. This is a well-established in vivo OIS model, where cells are proliferative close to the tumor stroma, but the suprabasal cells (closer to the surface) are non-proliferative differentiated/senescent cells. Dec1, a marker of senescence, is strongly positive in the non-proliferative area in both the nuclei and cytoplasm (A). The dashed red line denotes the basement membrane. Between the proliferative area and the senescent area, prominent perinuclear Golgi apparatus (GA) (GM130) are present. Perinuclear compartmentalization of mTOR is observed adjacent to the prominent GA, consistent with Ras-induced senescent IMR90 cells (B). In the same area, lysosomes (Lamp2) and autophagic vesicles (LC3) are enriched coincidentally (C). (**D** and **E**) Representative immunohistochemical images of serially sectioned normal mouse back skin (control) for indicated proteins. The bracket denotes epidermis.

Supplemental fig. S9

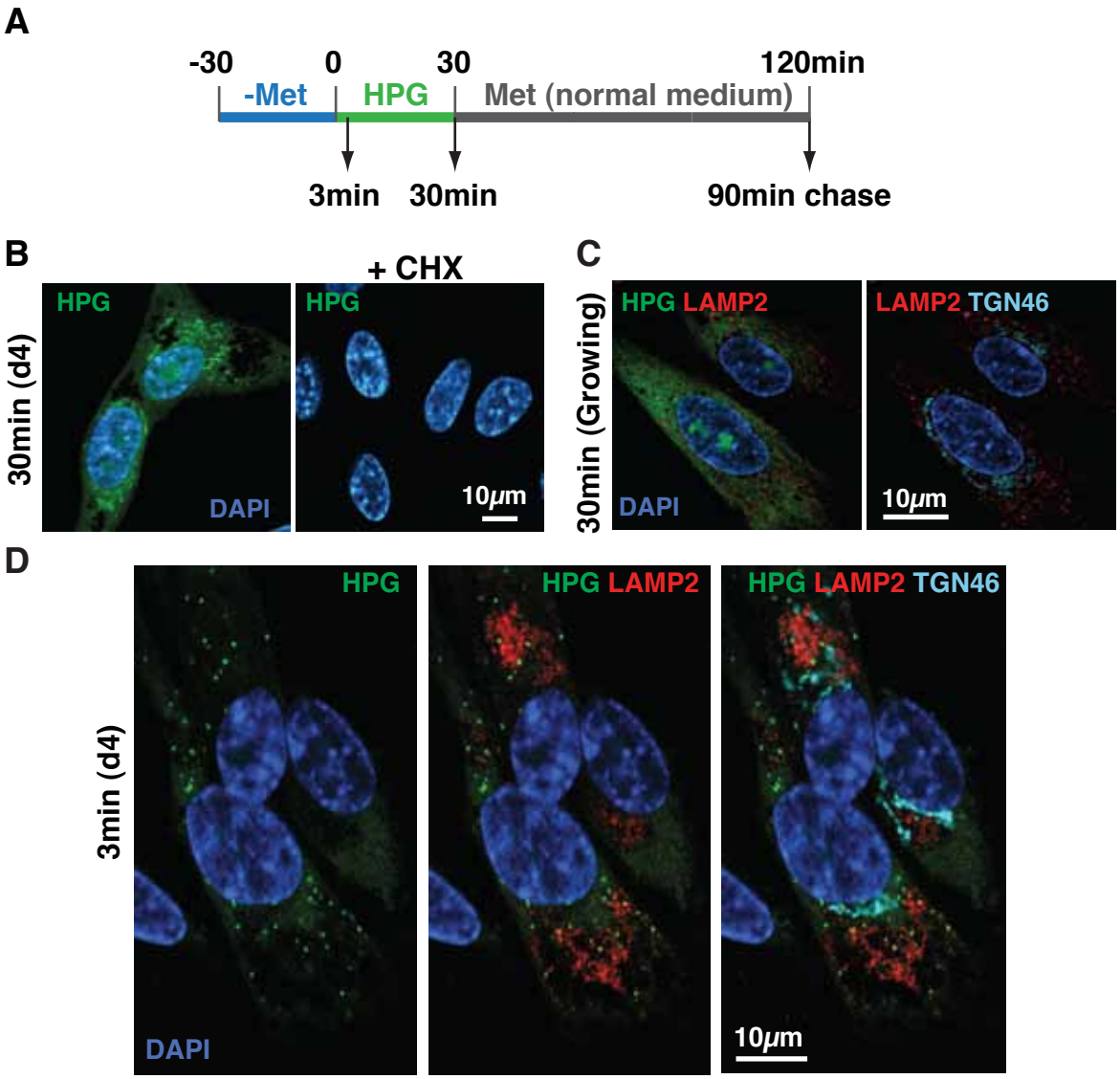

fig. S9. Visualization of nascent protein synthesis during Ras-induced senescence. (**A**) Experimental design. Cells were pre-cultured for 30min in methionine (Met) free medium, before metabolic labelling with a reactive (Click-iT) methionine analogue, L-homopropargylglycine (HPG). (**B**) HPG is incorporated into nascent proteins in Ras-induced senescence cells (d4). In control cells, an inhibitor of protein translation, cycloheximide (CHX, 25 μM) was added 30 min before HPG labeling. (**C**) Thirty min labelling with HPG in normal growing IMR90 cells (compare to Fig. 2F). Proteins were immunolabeled as indicated. (**D**) Short-term (3 min) labeling of HPG. Nascent protein was not yet colocalized with the TGN, but occasionally exhibited a punctate pattern, which was spatially associated with the TASCC.

Supplemental fig. S10

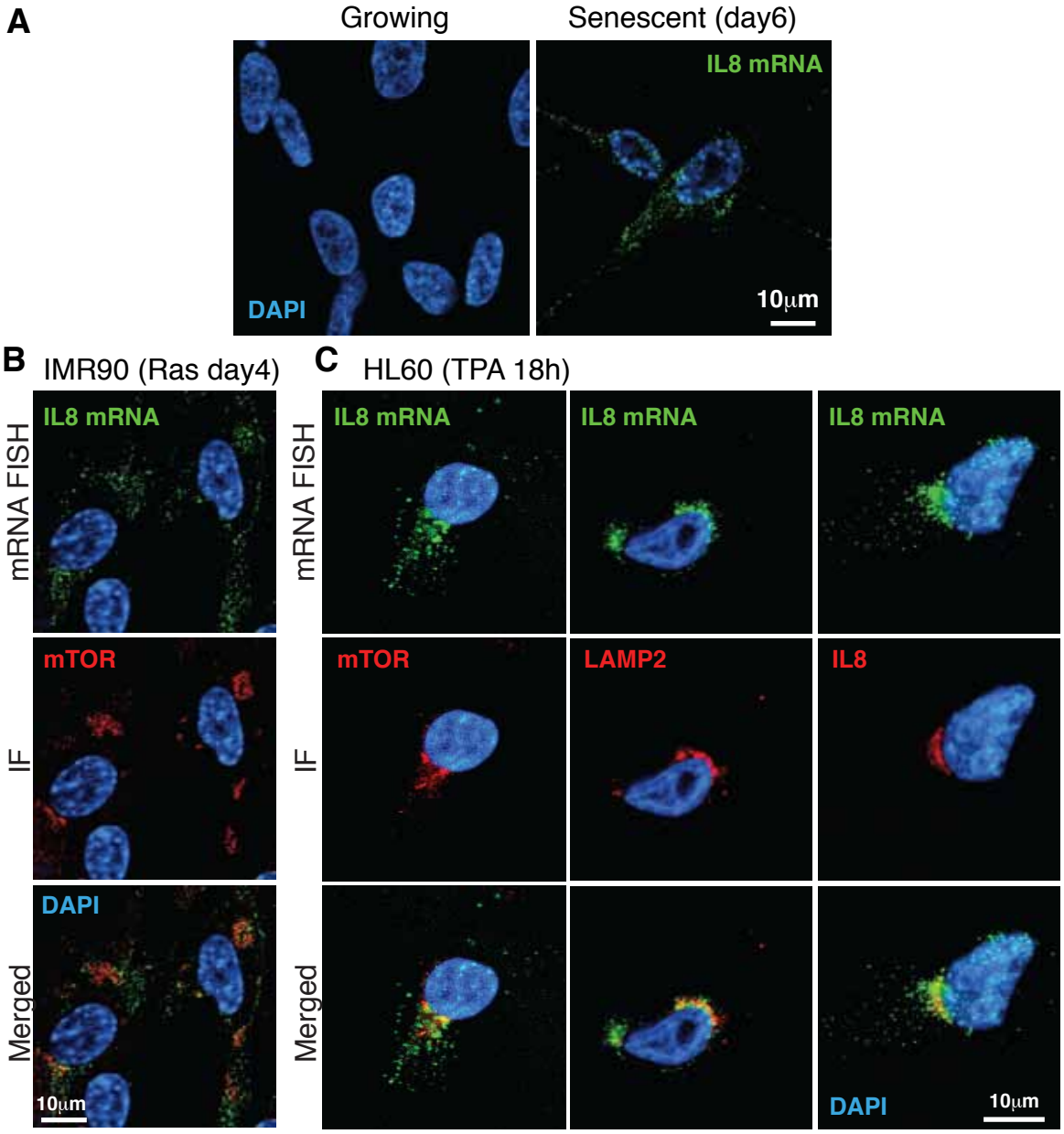

fig. S10. Spatial relationship between *IL8* mRNA and the TASCC in IMR90 and HL60 cells.

(**A**) Specific detection of *IL8* mRNA by mRNA FISH in day 6 Ras-induced senescent IMR90 cells. Representative confocal microscopy images are shown. (**B**) Representative confocal images of immuno-FISH, in which *IL8* mRNA is associated with marginal regions of the TASCC (mTOR IF). (**C**) Representative confocal images of immuno-FISH for mTOR, LAMP2, or IL8 proteins with *IL8* mRNA in TPA treated (18 h) cells. The spatial association between *IL8* mRNA and the TASCC was more pronounced in differentiating HL60 cells, where the process is shorter and quicker than Ras-induced senescence. IF, immunoflurorescence.

Supplemental fig. S11

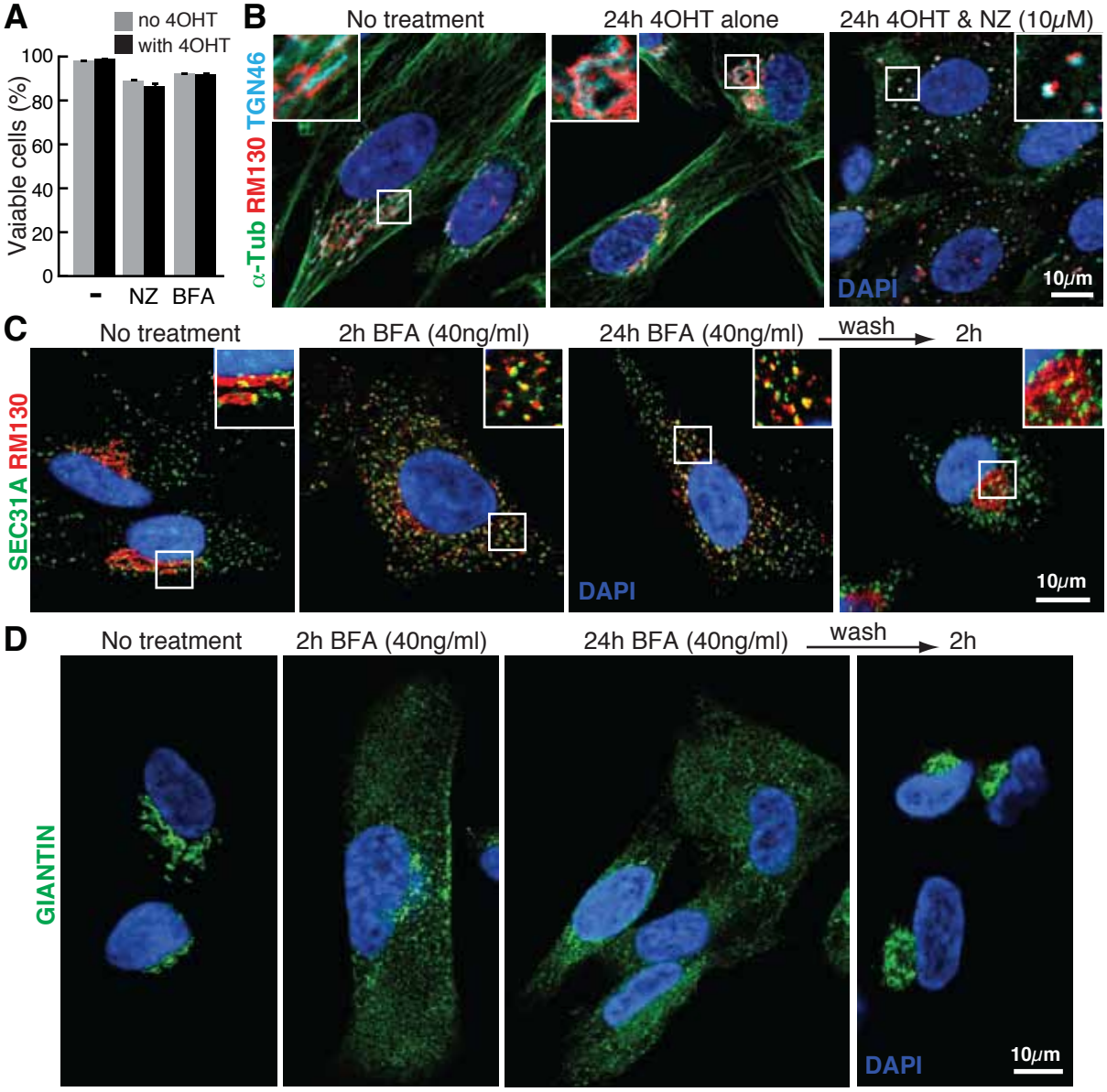

fig. S11. Validation of the long-term effect of nocodazole and brefeldin A in IMR90 cells.
(**A**) Cells were largely viable after long-term treatment with Brefeldin A (BFA) or Nocodazole (NZ). ER:Ras-IMR90 cells were treated with either no drug, 40 ng/ml BFA, or 10 μM NZ in the presence of 4OHT for 24 h (see Fig. 3B). The viability of cells was assessed by trypan blue exclusion. Values represent the mean ± SE (n=3). (**B**) Mini-stacks formation after 24h treatment of high dose (10 μM) NZ. Confocal images of immunofluorescence for α-tubulin (α-tub), RM130 (cis-Golgi network marker), and TGN46 (TGN) in cells treated as indicated. In the presence of high dose (10μM) NZ, microtubules were destabilized and the GA was fragmented, while Golgi mini-stacks were intact (magnified in the inset). (**C**) Relocation of RM130 (also called GMAP210) to ER-exit sites upon BFA treatment. Representative confocal images for SEC31A and RM130 in cells treated as indicated. SEC31A, a component of the COPII complex, is used as a marker of ER-exit sites. Although the distribution of RM130 tended to show more perinuclear pattern in 24h treatment compared to short-term (2h) treatment, the punctate RM130 pattern was still associated with ER-exit sites. In addition, GA was readily reformed after washing away BFA. (**D**) Representative confocal images for GIANTIN, another cis-Golgi marker, which is known to accumulate in ER after BFA treatment.

Supplemental fig. S12

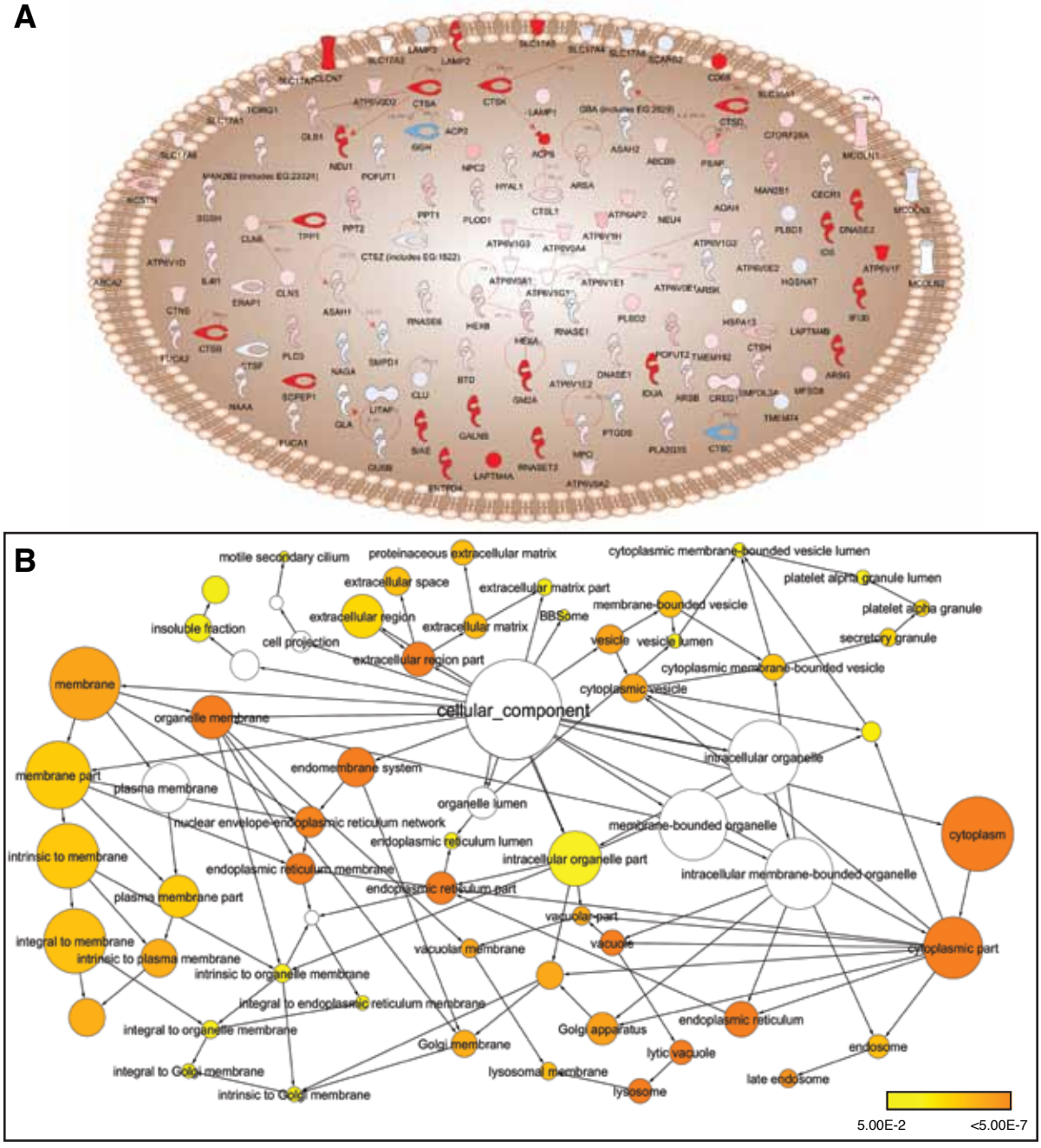

fig. S12. Lysosomal gene profile and network representation of 'cellular component' ontology enrichment

(**A**) Graphical representation of lysosomes at day 4 Ras-induced senescence. The intensity of the color of the molecule indicates the degree of up- (red) or down- (blue) regulation of gene expression. The genes colored dark red and blue are at least 1.5 fold up- or down-regulated, respectively. (**B**) Network representations of 'cellular component' ontology analysis of upregulated genes at day 4 after Ras-induction, where the diameter of the node is proportional to the number of genes represented by that ontology and the intensity of the color is proportional to functional enrichment.

Supplemental fig. S13

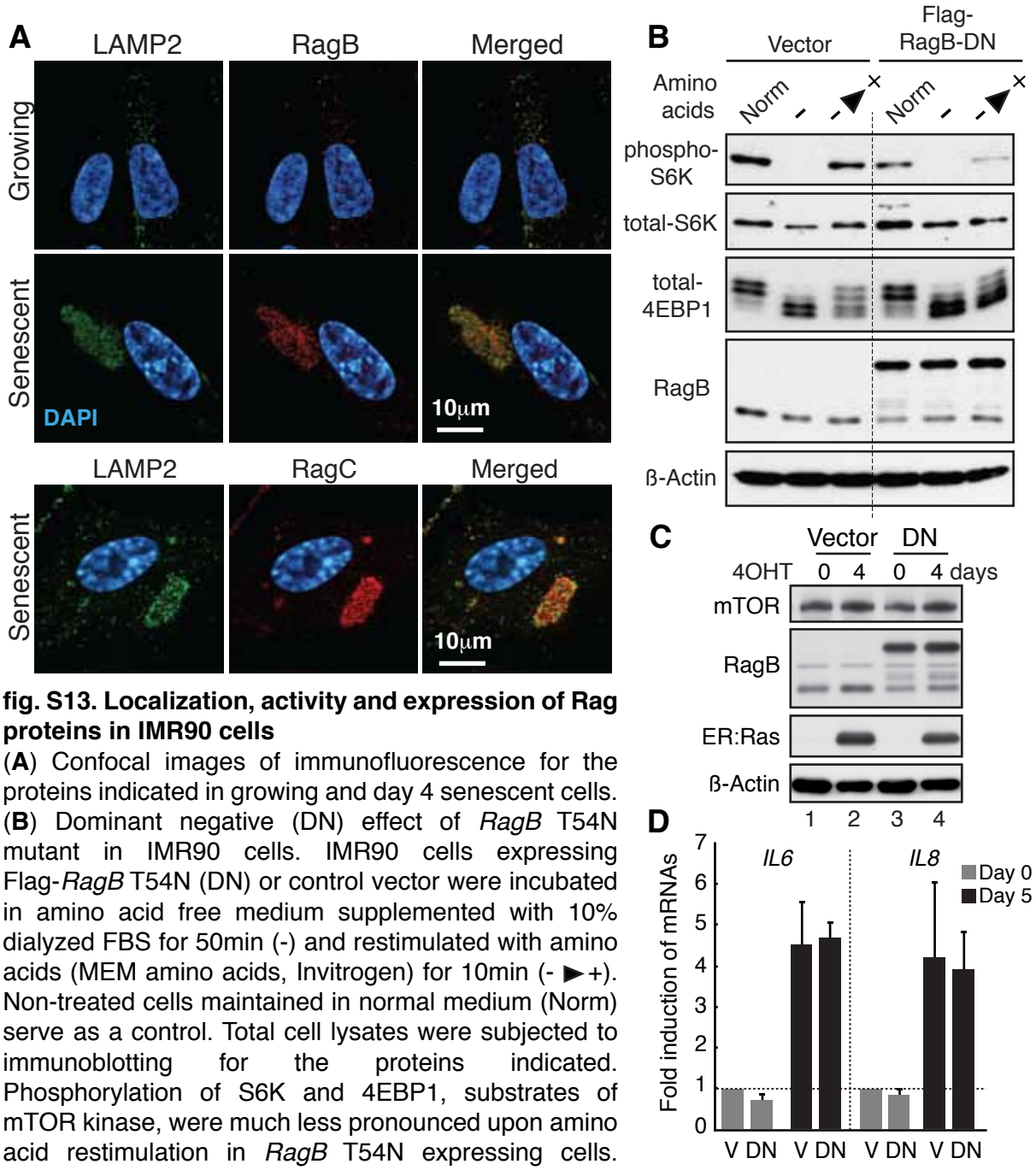

fig. S13. Localization, activity and expression of Rag proteins in IMR90 cells

(**A**) Confocal images of immunofluorescence for the proteins indicated in growing and day 4 senescent cells. (**B**) Dominant negative (DN) effect of *RagB* T54N mutant in IMR90 cells. IMR90 cells expressing Flag-*RagB* T54N (DN) or control vector were incubated in amino acid free medium supplemented with 10% dialyzed FBS for 50min (-) and restimulated with amino acids (MEM amino acids, Invitrogen) for 10min (- ►+). Non-treated cells maintained in normal medium (Norm) serve as a control. Total cell lysates were subjected to immunoblotting for the proteins indicated. Phosphorylation of S6K and 4EBP1, substrates of mTOR kinase, were much less pronounced upon amino acid restimulation in *RagB* T54N expressing cells. (**C**) Inhibition of Rag GTPase activity did not affect total mTOR levels. Immunoblot analyses for indicated proteins in ER:Ras-IMR90 cells expressing vector or Flag-*RagB* T54N (DN) at the indicated time points after Ras-induction. Compare lane 2 to lane 4. (**D**) RagB-DN expression did not cause any significant changes in the mRNA levels of IL6 or IL8. Levels of the indicated mRNAs were assessed by real-time quantitative PCR (qPCR) at the indicated time points after Ras-induction. *β-Actin* was used as the internal control. qPCR data were normalized to vector expressing growing cells (mean ± SEM; n=3).

Supplemental fig. S14

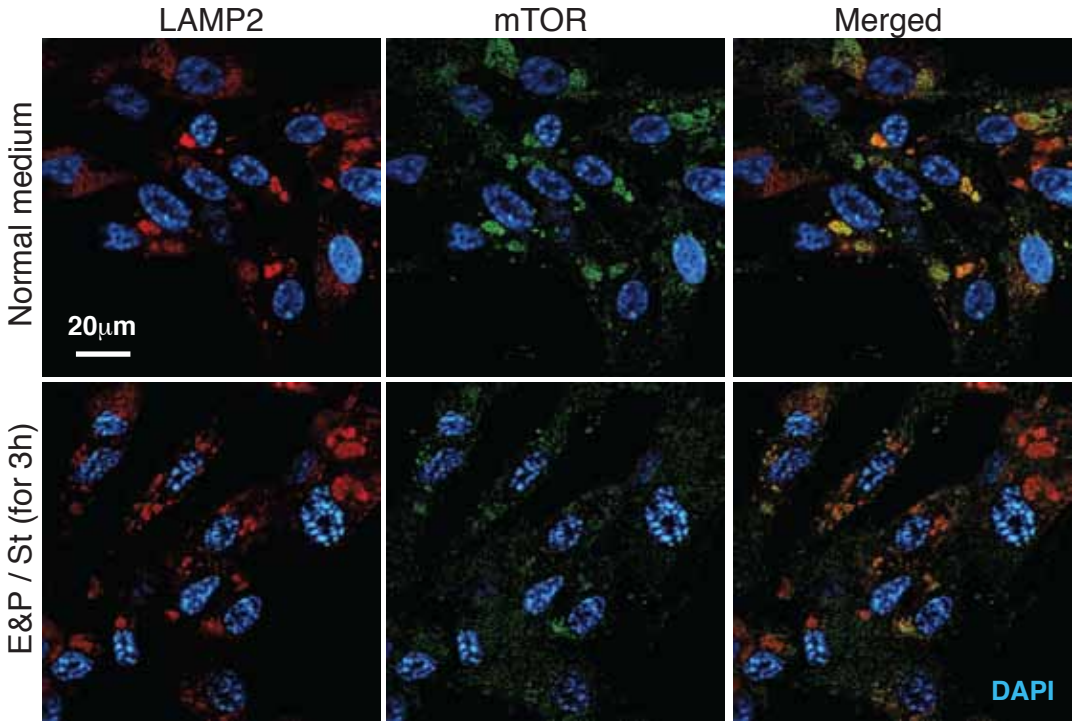

fig. S14. Effect of amino acid depletion on mTOR enrichment in LAMP2-compartments.
Confocal microscopy images of immunofluorescence for the proteins indicated in the conditions described in Fig. 4C. E&P, 10μg/ml E64d and 25μg/ml Pepstatin A (lysosomal protease inhibitors); St, amino acid-free medium supplemented with 10% dialyzed FBS.

Supplemental fig. S15

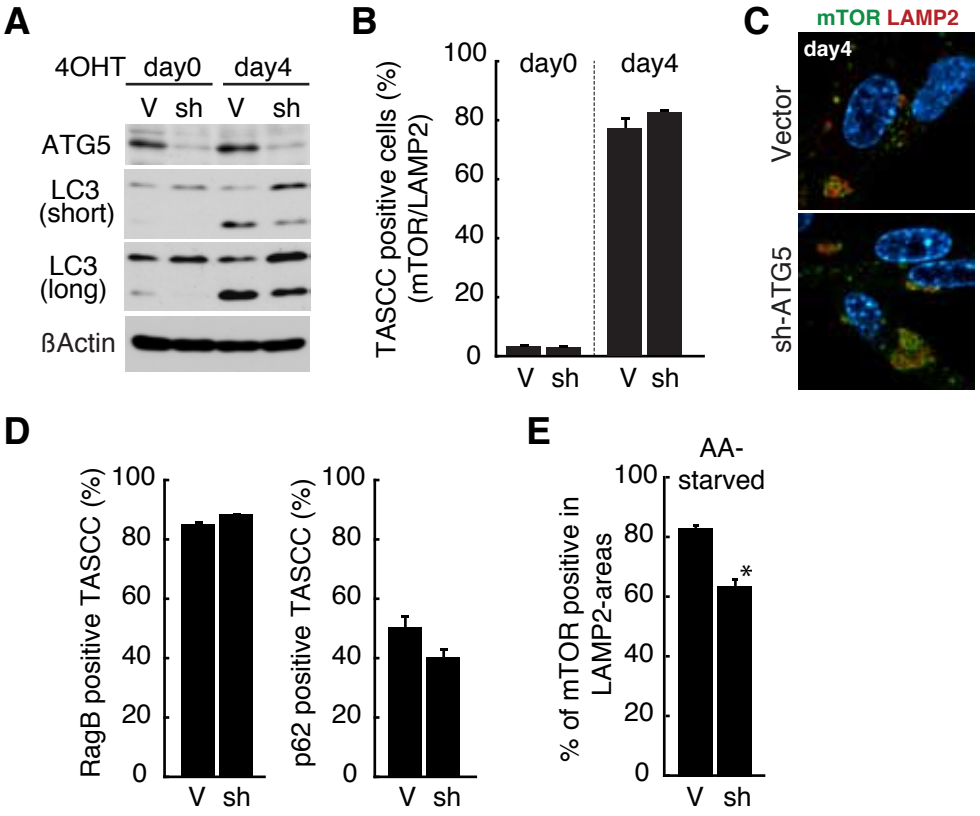

fig. S15. Effect of retroviral mediated short hairpin (sh)-ATG5 on TASCC formation
(**A**) Immunoblot analysis for indicated proteins. ER:Ras IMR90 cells expressing vector (V) or sh-ATG5 (sh) were given 4OHT for the number of days indicated. (**B** to **D**) sh-ATG5 alone does not significantly affect TASCC formation at day 4. Local enrichment of the proteins indicated was assessed by immunofluorescence. (**E**) sh-ATG5 inhibits mTOR enrichment in LAMP2-compartments in amino-acid free medium. ER:Ras cells (day 4) expressing vector (V) or sh-ATG5 (sh) were incubated with amino acid (AA)-free medium supplemented with 10% dialyzed FBS (St) for 3h. mTOR enrichment in the TASCC was assessed by immunofluorescence. Values are mean ± SEM; n=3 (B, D, and E). $*P < 0.01$.

Supplemental fig. S16

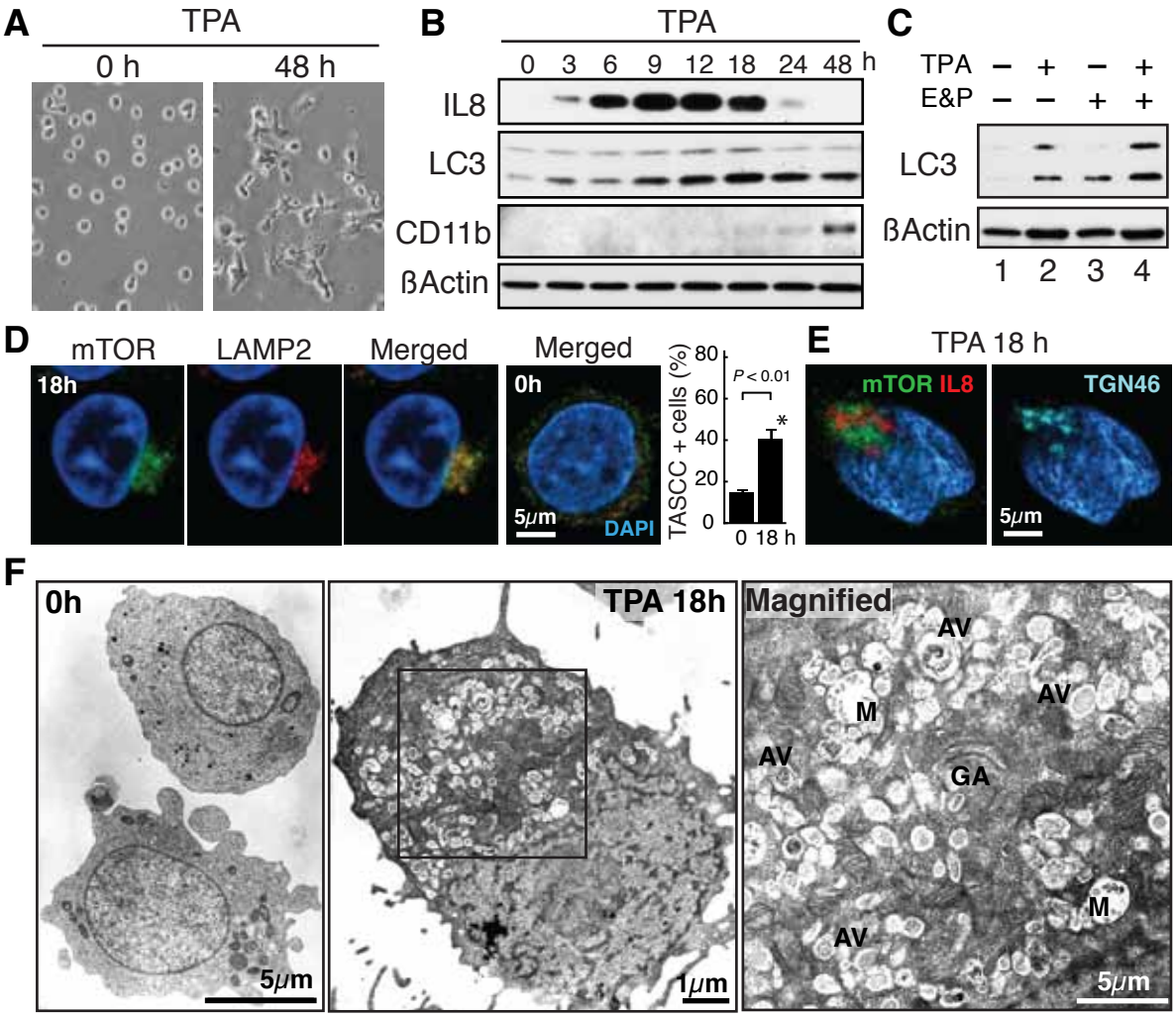

fig. S16. TASCC formation during macrophage-like differentiation in HL60 cells. (**A**) Phase contrast images of HL60 cells non-treated or TPA (30 nM) treated for 48 h. (**B**) Acute induction of IL8 and autophagy during macrophage-like differentiation of HL60 cells. Immunoblotting for indicated proteins. CD11b is a macrophage marker. (**C**) Autophagic flux is intact in differentiating HL60 cells. After 18 h TPA treatment (or no treatment), E&P (10 μg/ml E64d and 25 μg/ml Pepstatin A) were added for additional an 3 h. (**D** to **F**) Confocal immunofluorescence for the proteins indicated (mean ± SEM; n=3) (D and E) and EM images of cells indicated suggest that IL8 synthesis is associated with TASCC formation during macrophage-like differentiation in HL60 cells. The region indicated by the rectangle is magnified. AV, autophagic vacuole; GA, Golgi apparatus; M; multivesicular body.

Supplemental fig. S17

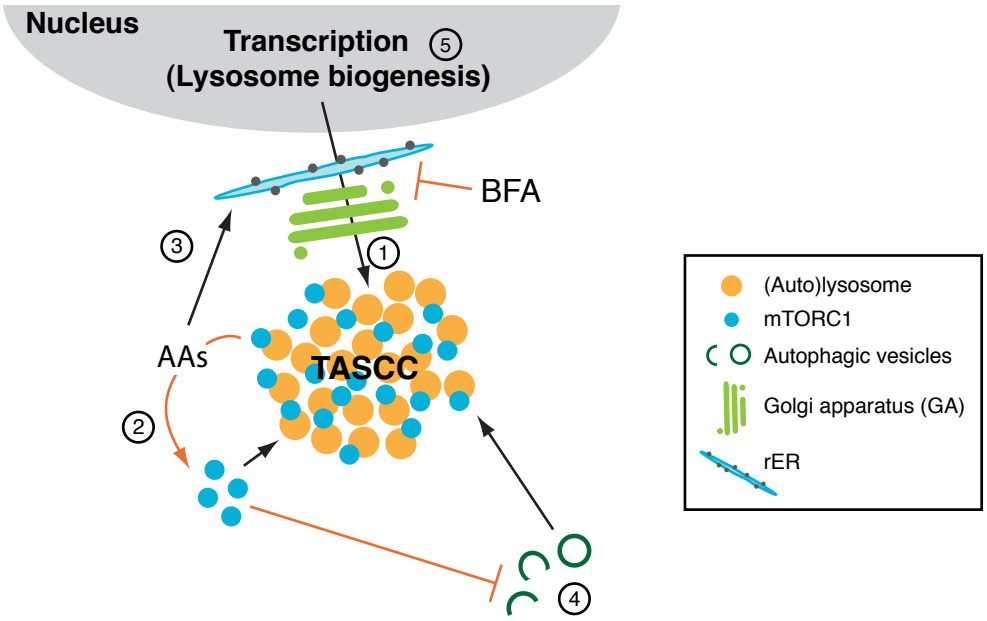

fig. S17. Model for TASCC formation.
The process of TASCC formation is progressive and composed of multiple 'modules'. The close spatial association between the TASCC and GA and the preventive effect of brefeldin A (BFA) on TASCC initiation suggest that de novo lysosome biogenesis is critical for TASCC nucleation (①); amino acids (AAs) derived from the TASCC contribute to mTOR recruitment to the TASCC via Rag GTPases (②); conceivably, the same amino acids might be efficiently used for protein synthesis through the nearby rER-GA system (this includes de novo lysosomal biogenesis as well), although how mTOR enrichment contributes to local translation is still unclear (③); autophagosome formation (negatively regulated by mTOR) occurs outside the TASCC (④), suggesting an interesting possibility that, by spatially separating the autophagosome formation and autolysosomal degradation, both autophagy and mTOR activities can be augmented. Finally, upregulation of lysosomal genes (and other genes involved in membrane biogenesis) would enhance the whole process (⑤). Black lines denote physical movement or directionality, while orange lines indicate signalling.

table S1.

Functional Annotation Cluster	Enrichment score	*P*-value	BH *P*-value	GO type
Lysosome	9.54	2.5e-10	4.1e-8	CC
Lytic vacuole	9.54	2.5e-10	4.1e-8	CC
Vesicle	5.30	4.8e-7	3.3e-5	CC
Secretory granule	5.30	7.3-5	1.8e-3	CC
Endoplasmic reticulum	4.52	3.4e-4	6.6e-3	CC
Extracellular region	3.79	6.4e-6	2.4e-4	CC
Membrane	4.04	1.5e-5	4.2e-4	CC
Vacuolar membrane	2.61	1.8e-3	2.5e-2	CC
Integral Golgi membrane	1.97	4.0e-2	2.9e-1	CC
Cytoplasmic vesicles	1.16	1.7e-2	1.7e-1	CC
Secretory Granule membrane	1.16	9.6e-2	4.9e-1	CC
Inflammatory Response	7.66	3.8e-7	1.3e-4	BP
Membrane	5.15	2.0e-7	2.3e-5	BP
Lipid Synthesis	2.16	3.1e-5	2.0e-3	BP
Sterol Biosynthesis	2.16	2.3e-3	5.0e-2	BP
Vesicle mediated transport	1.95	1.5e-2	3.2e-1	BP
Regulation of hydrolase activity	1.54	4.3e-3	1.6e-1	BP
Fatty Acid Biosynthesis	1.49	2.3e-2	3.8e-1	BP

CC - Cellular Compartment Ontology

BP- Biological Process Ontology

table S1. Functional analysis of upregulated genes at day 4 Ras-induced senescence.

Gene Ontology analysis was performed using the NIH DAVID software. Enriched and statistically significant ‘cellular compartment’ and ‘biological process’ ontologies for upregulated genes are shown. Enrichment score, *P*-value, Benjamini-Hochberg (BH) FDR adjusted *P*-value and ontology type are given for each ontology term.